Dual-Level Direct Dynamics of the Hydroxyl Radical Reaction with Ethane and Haloethanes: Toward a General Reaction Parameter Method

S. Sekušak,*,† M. G. Cory,‡ R. J. Bartlett,‡ and A. Sabljić†,§

Institute Ruđer Bošković, Department of Chemistry, P.O. Box 1016, HR-10001 Zagreb, Republic of Croatia, Quantum Theory Project, Departments of Chemistry and Physics, University of Florida, Gainesville, Florida 32611, and Institut fuer Meterologie und Klimaforschung, Forschungzentrum, Karlsruhe/Universitaet Karlsruhe, D-76021 Karlsruhe, Germany

Received: June 29, 1999; In Final Form: October 5, 1999

The dynamics of hydroxyl radical reactions with ethane, fluoroethane, and chloroethane have been examined in terms of variational transition state theory augmented with multidimensional semiclassical tunneling corrections. Differences in reactivity for hydrogen abstraction from both the primary and the secondary carbon atoms are examined in terms of energetic and entropic effects on the location of the dynamical bottleneck. Interpolated variational transition state theory is used to calculate reaction rate constants at the [G2(MP2)//MP2/6-31G(d,p)]/SCT level of theory. A vibrational-mode correlation analysis is performed; i.e., the character of the vibrational modes are identified as a function of the reaction coordinate and a statistical diabatic model is used to provide qualitative analysis of a possible vibrational-state specific chemistry for this reaction. A significant enhancement of the reaction rate is predicted for the excitation of the pertinent C−H stretching mode of the reactant hydrocarbon molecule. The standard PM3 Hamiltonian is reparametrized (via a genetic algorithm) to obtain reliable semiempirical potential energy surfaces for the reaction of ethane with the OH radical. The specific reaction parameters (SRP) so obtained are then used to predict the reaction rate constants for both the fluoroethane and chloroethane abstraction reactions. The temperature dependence of the rate constants calculated at the [G2(MP2)//MP2/6-31G(d,p)///PM3-SRP]/μOMT level of theory are compared with those of experiment and are found to be in very good agreement. (The computed rate constants differ from experiment by, at most, a factor of 2.5.) We demonstrate that the specific reaction parameters can be used for analogous reactions of the same mechanism, implying a general reaction parameter set (GRP) for related molecules. Perhaps reaction rates for larger hydrocarbons (that are of interest in atmospheric and combustion chemistry) can be obtained reliably at low computational cost.

Introduction

Abstraction of a hydrogen atom by the hydroxyl radical is an important rate-determining step in the combustion (and atmospheric) chemistry of hydrocarbons[1,2] and has therefore attracted considerable attention from both experimentalists[3,4] and theoreticians alike.[5−8] Previously, ab initio molecular orbital methods have been used to study the potential-energy surfaces describing H abstraction from the three simplest hydrocarbons; i.e., methane,[5a−e,6a,6b] ethane[6c,7a,8a] (their halogenated analogues[5j,7b,8]), and propane.[6e] Only recently have theoretical kinetics studies for these reactions become available.[9−11] The hydrogen abstraction reactions of propane (and its isotopic derivatives[6e]) have recently been studied by the dual-level approach to direct dynamics.[12] In this work H abstraction from ethane,[6c,8e] fluoroethane,[8e] and chloroethane[8e] has been studied using variational transition state theory[9−13] augmented with multidimensional semiclassical tunneling corrections.[9,11]

One objective of this work is to compare hydrogen abstraction reactions from the primary and secondary carbon atoms in the halogenated ethanes, and to examine entropic effects on the position of the dynamical bottleneck. Accounting for quantum mechanical tunneling may prove important[14] for these hydrogen transfer reactions; thus, a second goal of this work is to obtain specific reaction parameters (by re-parametrizing the semiempirical PM3-NDDO Hamiltonian) to carry out multidimensional tunneling calculations within both the small[11,15] and the large curvature approximations.[11,16]

For the halogenated ethanes hydrogen atoms can be abstracted from either the primary or the secondary carbon atoms. For primary abstraction two different transition-state (TS) structures were found,[8b] and for secondary abstraction a single TS structure was located. (In Figure 1 we define the various transition states.) Therefore, at least three different reaction paths are possible for the OH radical reaction with fluoroethane and chloroethane. Abstraction from the secondary carbon was found to be energetically favored and is in agreement with Atkinson's empirical model that predicts hydrogen abstraction from the secondary carbon atom to contribute 80% to the overall reaction rate.[3d] However, it was also found[8b,8f] that abstraction from the primary carbon atom is governed by through-space van der Waals interactions between the hydroxyl hydrogen and the halogen atom. This interaction has the effect of lowering the barrier heights by ≈30%. In this study we investigate how such interesting interactions, as well as how the entropy, affect the

† Institute Ruđer Bošković.
‡ Quantum Theory Project.
§ Institut fuer Meterologie und Klimaforschung.

10.1021/jp9922256 CCC: $18.00
Published on Web 12/04/1999

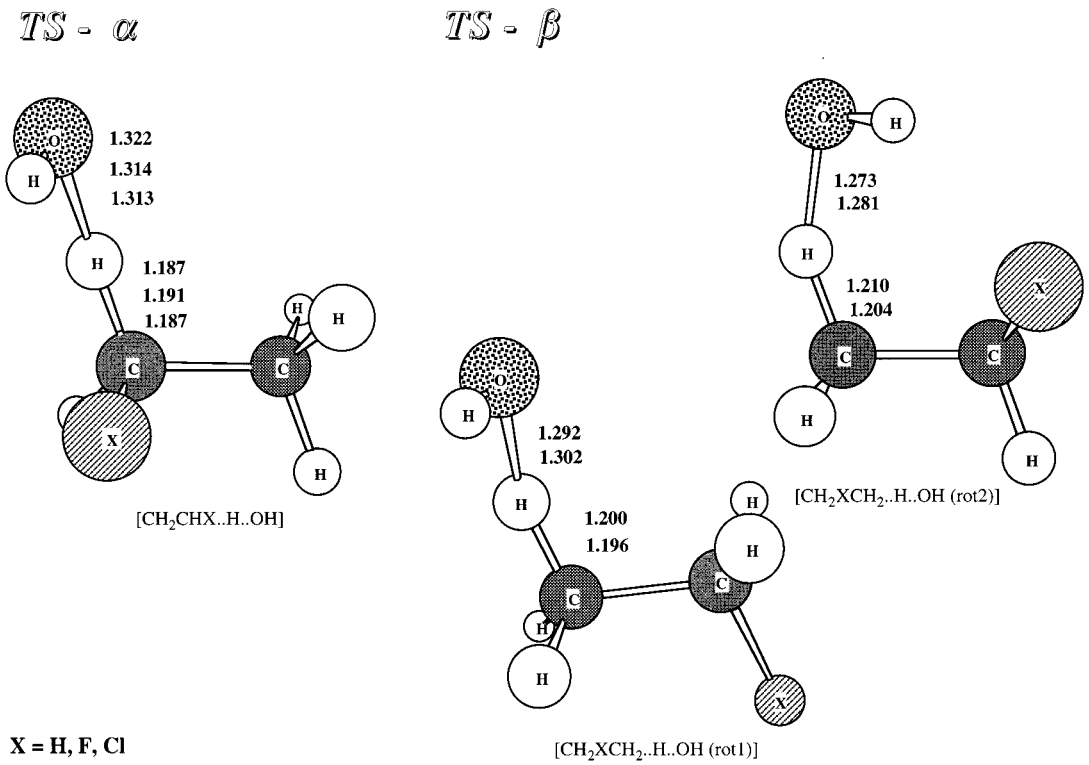

Figure 1. Reactive geometrical parameters of the transition state structures for reactions R_H, R_F, and R_{Cl} calculated at the MP2/6-31+G(d,p) level of theory.

overall reaction rate. (Below we define our labeling scheme for the various reactions.)

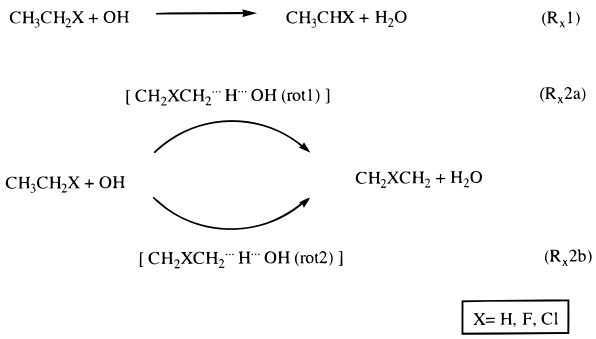

In a previous study[8b] a detailed analysis of the reaction-path dynamics of abstraction from the favored secondary carbon atom for both fluoroethane and chloroethane was performed. The reaction rate constants were calculated using interpolated variational transition state theory (IVTST)[9,11] and small curvature tunneling (SCT) corrections.[11,15] In the present paper reaction rates have been calculated for abstraction from the primary carbon of fluoroethane, again using IVTST, and the site-specific differences in reactivity are discussed in terms of the energetic and entropic factors. (Entropic effects on the location of the dynamical bottleneck should be considered whenever the intrinsic barrier is small and the potential is relatively flat in its vicinity,[17] a scenario which characterizes the reactions investigated in this work.) We also employed a statistical diabatic model to provide a qualitative analysis of the possible vibrational-state specific chemistry of hydrogen abstraction from ethane, fluoroethane and chloroethane.

Another goal of this paper is to calculate the rate constants via a dual-level approach to direct dynamics[12] through the use of the semiempirical PM3-NDDO Hamiltonian[18] reparametrized to specifically describe the reaction mechanism of interest;[9] i.e., we used a set of specific reaction parameters (SRP). Dual-level dynamics based on such semiempirical hyper-surfaces have been successfully applied in the determination of hydrogen transfer reaction rate constants in the past.[6e,20] The specific reaction parameters we obtained for the ethane abstraction reaction are then tested on the analogous fluoroethane and chloroethane abstraction reactions as a step toward understanding how to generate general reaction parameters (GRP); i.e., a set of parameters capable of yielding quantatatively correct rates when applied to analogous molecular systems undergoing the same reaction. Examples of the applicability of our SRP/GRP parameters for determining rates for larger hydrocarbons are also given.

Computational Methods

Electronic Structure Calculations. The minimum energy paths (MEP) for reactions R_F2a and R_F2b have been calculated using second-order perturbation theory (MP2=MBPT(2)) relative to a UHF reference;[21] i.e., at the MP2(full)/6-31+G(d,p) level of theory,[22] in steps of $0.1a_0$ using the Gonzalez−Schlegel IRC algorithm.[23] The reaction coordinate *s* is given in isoinertial coordinates with a scaling factor of 1 amu. The force constant matrixes were computed in steps of $0.2a_0$ along the MEP.[24] For the open-shell systems spin projection[25] was used to eliminate spin contamination arising from states with spin (s+1) to (s+4). These data were used together with previously published results for the R_H1, R_F1, and $R_{Cl}1$ reactions[8e] and with G2(MP2)[25] energetics (computed for all stationary points[8e]) for the dynamics calculations described below.

To obtain an inexpensive method for the calculation of reliable potential energy hypersurfaces the PM3 Hamiltonian[18] was reparametrized as described in the next section. The necessary structural, vibrational, and thermodynamic data were obtained from an interface to MOPAC 5.07mn.[27] Electronic

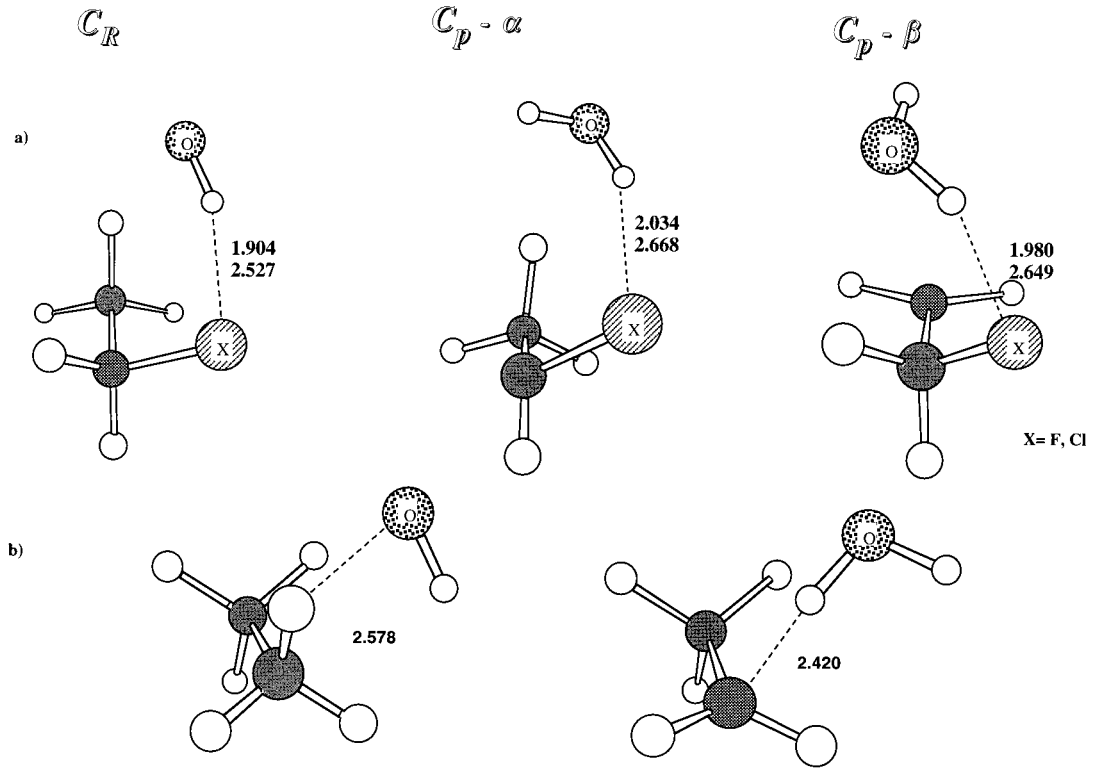

Figure 2. Geometrical parameters of the van der Waals complexes that are found on the reactant and the product sides of the MEP, calculated for the R_H, R_F, and R_{Cl} reactions at the MP2/6-31+G(d,p) level of theory.

structure calculations were done using the GAUSSIAN94 quantum mechanical suite of programs.[28]

Ab initio data were used to obtain reaction rate constants in terms of interpolated variational transition state theory[9−11] and for the validation of the PM3-SRP potential energy surface.

NDDO Parametrization. The semiempirical PM3 Hamiltonian[18] was re-parametrized to reproduce to the degree possible high-quality G2(MP2)//MP2/6-31G(d,p) structural and energetic data at three stationary points on the potential energy hyper-surface describing the reaction of ethane with OH. This parameter optimization was carried out using GaFortran 1.6.4,[29] a global, genetic algorithm (GA)[30] based, optimization program. In our case the NDDO parameters to be varied were all one- and two-electron integrals with the bounds of the variation set to ±10% of each parameter's initial value. The fitness (error) function to be minimized by the GA is defined as the sum of the following terms: (i) weighted squared relative differences between reference and predicted forward barriers, (ii) weighted squared relative differences between reference and predicted reaction enthalpies, and (iii) a standard penalty for each ab initio structure whose NDDO-SRP gradient is not zero. The squared relative differences are defined as $(((q_i^{calc} - q_i^{ref})/q_i^{ref}) \times 10^2)^2$. The barrier heights and reaction enthalpies are weighted the same. The squared sum of the individual NDDO-SRP gradient errors is weighted such that it is not allowed to obscure the influence of the energetic errors. The gradient of the TS is preferentially weighted by a factor of 3 relative to the other structures. For the cases where either the calculated barrier height is negative, or the reaction enthalpy is positive, or when the SCF procedure will not converge, the fitness of the parameter set is given an extremely large value, thus removing the possibility of the parameter set being propagated further. The fitness function is then minimized using the GA. The specifications used in conjunction with running the GA were a uniformly distributed starting generation of 200 individuals, 10 bits per parameter, a uniform crossover probability with a crossover rate of 0.5 and a mutation probability of 0.005. The optimization was considered converged when the returned value of the fitness function had stabilized and the individual errors were acceptably small. This turned into an art form.

Reaction Rate Calculations. Reaction rate constants were calculated by interpolated variational transition state theory with interpolated corrections (IVTST-IC).[12] Further, both the zero-curvature tunneling[11] (ZCT) correction and the small curvature tunneling[11,15] (SCT) correction were included, as quantum mechanical tunneling can be important when H is involved. Dual-level dynamics[12] including the SCT correction, the large curvature tunneling[11,16] (LCT) correction and the microcanonical multidimensional tunneling approximation[31] (μOMT) correction, was also used.

IVTST-IC. The IVTST-IC approach was carried out in two steps. First, we performed electronic structure calculations to obtain the energies, gradients, and Hessians of the reactants, products, transition state and 20 other points along the reaction path. This was done at the MP2(full)/6-31G(d,p) level of theory. Then, the energetics previously calculated at the G2(MP2) level of theory[8e] were used to interpolate corrections to the lower level energetics, a three-point Lagrangian interpolation was used as implemented in the Polyrate suite of programs.[32] The vibrational normal modes were correlated diabatically[33,8e] since it was shown that the entropy and the free energy curves can be evaluated incorrectly if an adiabatic interpolation is employed. Quantum mechanical tunneling effects were included through the SCT correction.

Direct Dynamics. Direct dynamics, within the dual-level dynamics scheme,[12] was also applied in this work. The potential energy hyper-surface necessary for the dynamics calculations was evaluated "on the fly"; i.e., dynamical quantities were calculated using the semiempirical electronic structure calculations for all required energies, forces, and Hessians, without

TABLE 1: The Energetics for the Reactions of OH with Ethane, Fluoroethane, and Chloroethane (kcal/mol)

reaction	ΔE_1	ΔE_2	ΔE_3	ΔE_4	$\Delta E^{\grave{a}}$	ΔH_r	E_a[a]	ΔH_r (exptl)[a]
ethane	−0.2	3.1	−21.1	0.5	2.9	−17.1	2.1−2.3	−19.0
$[CH_3CHFH\cdots O\cdots H]$		4.8	−22.6	1.3	2.1	−19.2		−18.7[b]
$[CH_2FCH_2H\cdots O\cdots H(rot1)]$	−2.7	7.0	−22.3	2.0	4.3	−15.3	1.5−2.3	−14.7[b]
$[CH_2FCH_2H\cdots O\cdots H(rot2)]$		6.0	−21.5		3.3			
$[CH_3CHClH\cdots O\cdots H]$		3.4	−23.6	1.2	1.1	−21.3		−21.2
$[CH_2ClCH_2H\cdots O\cdots H(rot1)]$	−2.3	5.7			3.4	−16.9	0.8−2.0	−17.1[b]
$[CH_2ClCH_2H\cdots O\cdots H(rot2)]$		5.1			2.8			

[a] Experimental data are referenced in the Methods section. [b] Values calculated at G2(MP2) level of theory.[8e]

the intermediacy of an analytic potential energy function.[9,34] The reaction path was computed using an Euler integrator[35] with a gradient step-size of 0.01 a_0 and the Hessian recalculated every 9 steps.[36] The information from the ab initio level was introduced into the semiempirical SRP surface by means of interpolated corrections (IC).[12] The geometries and vibrational frequencies were corrected with those calculated at the MP2-(full)/6-31G(d,p) level, and the energetics were further improved using the G2(MP2) results. The vibrational frequencies were corrected using the interpolated-corrections-based-on-ratios scheme[32] (ICR) since it gave a reasonable interpolation for the vibrational frequencies for all studied reactions. The energy along the reaction path $V_{MEP}(s)$ was improved by fitting the ab initio results for the reactants, products, and saddle point to an Eckart function.[12,32] The improved method[37] where the correction is approximated by the difference between two Eckart functions, one fitted to the lower-level $V_{MEP}(s)$ and the other fitted to the higher level energies for the reactants, products, saddle point, and the imaginary frequency of the saddle point, was not used since it failed to approximate the right shape of the higher level $V_{MEP}(s)$. This has been previously observed in the reaction of CH_4 with O.[38] The range parameter L for the Eckart function was gained from a four point fit using the reaction complexes on both sides of the MEP in the interpolation. It should be pointed out here that pre-reaction complexes were not used for correcting $V_{MEP}(s)$ since the values of the reaction coordinate for the reactant side complexes were not determined due to the convergence problems of the IRC algorithm.[8e] However, it could be expected that fitting the MEP to a more realistic $A + B \rightarrow (AB)_{CX} \rightarrow (AB)^{TS} \rightarrow (CD)_{CX} \rightarrow C + D$ shape[12a] would make it narrower thus increasing the tunneling corrections and the rate constants correspondingly. This effect was partially taken into account by calculating the range parameter L for the Eckart function with respect to the energies of the prereaction complexes, while in the previous work L was fitted with respect to reactant and product energies.[8e] Tunneling was included through the microcanonical optimized multidimensional tunneling approximation with the exit channel for the large-curvature tunneling restricted to the vibrational ground state. Tunneling into excited states was investigated and was found to make a negligible contribution.

According to the standard notation of dual-level dynamics[6d] the full notation for IVTST-IC and direct dynamics rate constants are given as G2(MP2)//MP2(full)/6-31G(d,p) and G2-(MP2)/MP2(full)/6-31G(d,p)///PM3-SRP, respectively. Throughout the rest of this paper we will use a shorthand notation, i.e., G2//MP2 for G2(MP2)//MP2/6-31G(d,p) and G2/MP2///SRP for G2(MP2)/MP2(full)/6-31G(d,p)///PM3-SRP. When tunneling corrections are included we use the labels (G2//MP2)/SCT and (G2/MP2///SRP)/μOMT.

The low-frequency modes that become imaginary along the reaction path due to the use of rectilinear coordinates were interpolated directly from the frequencies of the transition-state, reactant and product structures in terms of the IVTST-0 treatment.[12a] The harmonic approximation is assumed for the calculation of the vibrational partition functions in all cases with the exception of the internal hindered-rotation of the OH group around the reactive $O-H_a$ bond. For this situation a hindered rotor[39] model was employed.

For vibrational-state selected rate constants the statistical vibrationally diabatic model[40] was employed. The main assumption of this model is that vibrational modes preserve their characteristic motions along the reaction coordinate. In this case the vibrational modes are correlated by maximizing the overlap of successive points on the reaction path. The expression for vibrational-state selected rate constants differs from the statistical form of the thermal rate only in the vibrational partition function for the selected mode. The vibrational partition function of mode i in state m is given by

$$q_i(m,T) = e^{-(1/2+m)h\omega_i/k_BT}$$

The dynamic calculations were carried out using the POLYRATE (version 7.8.1[32]) and MORATE (version 7.5[41]) programs.

Experimental Results. The reaction of ethane with the OH radical has been studied with several experimental techniques and the reaction rate constants for a wide range of temperatures have been reported.[3,42] Unfortunately, for the analogous fluoroethane and chloroethane reactions only a few such measurements[3d,43,44] exist. From their temperature dependence Arrhenius activation energies (E_a) have been obtained, and for the R_H reaction the range of E_a was found to fall between 2.1 and 2.3 kcal/mol. For the R_F reaction the range is 1.5−2.3 kcal/mol and for the R_{Cl} reaction 0.8−2.0 kcal/mol. Reaction enthalpies for the R_H and $R_{Cl}1$ reactions are calculated from experimental heats of formation.[45]

Results

Primary and Secondary Abstractions. In a previous study all stationary points for the R_x1 and the R_x2 reactions were determined[8a,8b] at the MP2/6-31G(d,p) level. (The important geometrical parameters of the computed transition-state structures are shown in Figure 1.) The reaction paths for the ethane abstraction reaction as well as for the favored abstraction from the secondary carbons of fluoroethane and chloroethane were also previously reported.[8e] Information about the geometry, frequency, and energy changes along the MEP were used to calculate the rates via the IVTST-IC method. (Energetics calculated at the G2(MP2) level of theory are given in Table 1.) It was shown that for the haloethanes hydrogen abstraction from the secondary carbon atom is energetically favored, although a significant lowering of the barrier height was found for the $[CH_2XCH\cdots H\cdots OH(rot2)]$ transition-state structures due

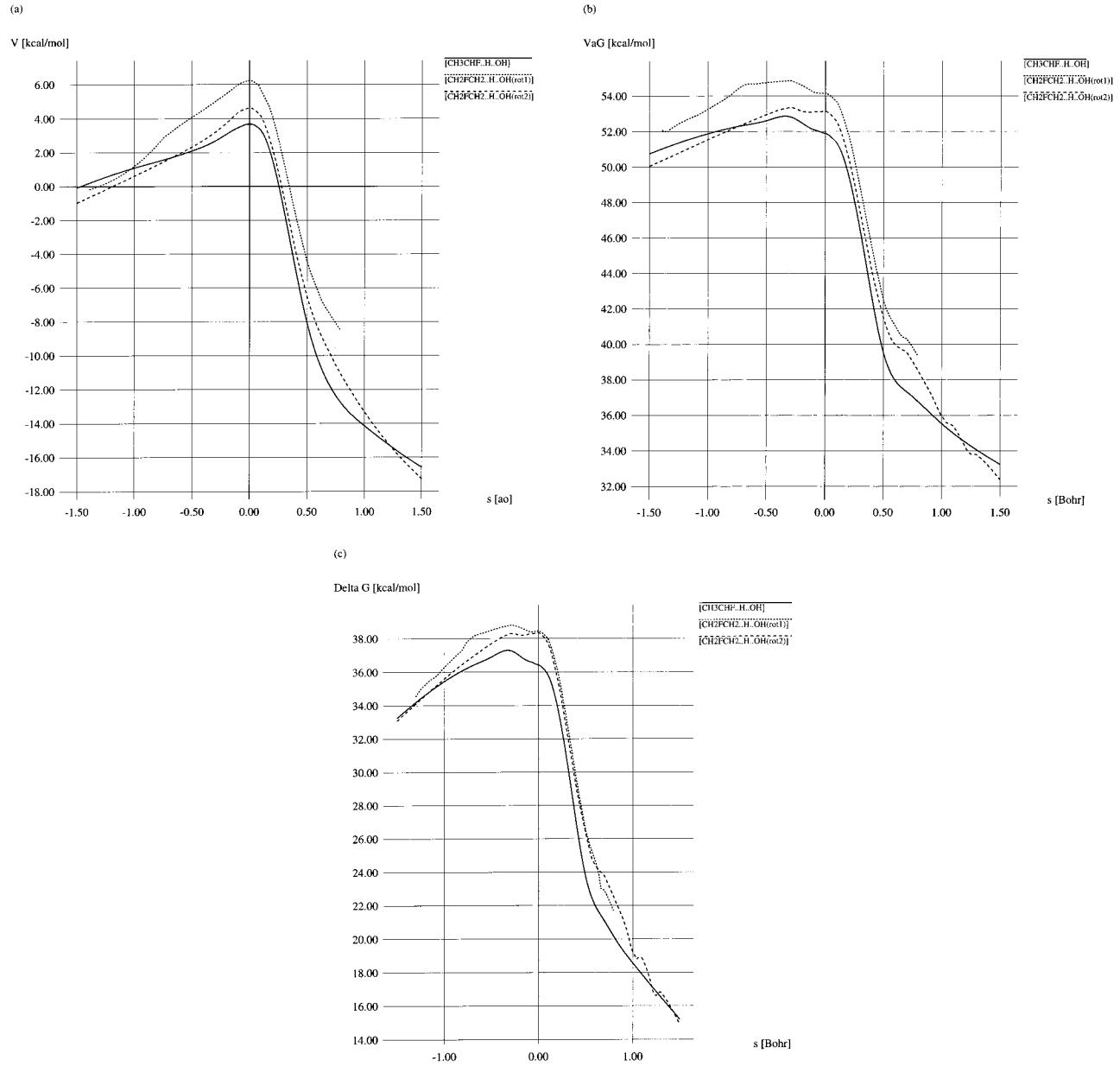

Figure 3. (a) The Born−Oppenheimer potential energy (V_{MEP}), (b) the vibrationally adiabatic ground-state potential energy (V_a^G), and (c) the free energy change along the reaction path for reactions R_F1, R_F2a, and R_F2b, at 298 K.

to the through-space interaction between the hydrogen atom of the OH radical and the halogen atom. Values ΔE_1 and ΔE_4 correspond to the stabilization energies of the van der Waals prereaction complexes that were found for all 5 reactions studied.[8f] In Figure 2 the important geometrical parameters are summarized.

The minimum energy paths were also calculated for the [CH_2-XCH···H···OH(rot1)] and [CH_2XCH···H···OH(rot2)] reaction pathways at the MP2/6-31G(d,p) level. This in order to compare energetic and entropic factors that govern hydrogen atom abstraction from both the primary and secondary carbon atoms in the fluoroethane abstraction reaction. Geometries and Hessians for generalized transition-state structures were calculated along the MEP as described in the Methods section. The resulting generalized normal modes were reordered by projecting the eigenvectors of each successive step onto those of the previous step, then connecting those with the largest contribution for a specific eigenvector. Due to strong mixing, the reordering and connection of the frequencies was not completely straightforward and some chemical intuition was needed to connect the frequencies reasonably. As in the case of the R_H1, R_F1, and $R_{Cl}1$ reactions, out of all $3N-7$ generalized normal modes, there are only two that change significantly during the reaction.[8e] These are the symmetric C−H stretching mode of the CH_2 group from which the hydrogen is abstracted and the symmetric O−H stretching mode of the product water molecule. The effect these particular frequencies have on the adiabatic ground-state potential energy as a function of position along the MEP is shown in Figure 3. The maximum of the ground-state vibrationally adiabatic potential energy curve appears at $s_*^{AG} = -0.2876a_0$ for reaction R_F2a and at $s_*^{AG} = -0.0026a_0$ for reaction R_F2b, this in comparison to $s_*^{AG} = -0.3429a_0$ for reaction R_F1. (It should be noted that a negligible variational shift is obtained for reaction R_F2b while for reaction R_F2a a significant, although smaller than that of the R_F1 reaction, variational shift is observed.) For the case of the R_F1 and the R_F2a reactions the shift of the maxima toward the reactants is due to the strong change in the $\nu(CH_2)$ mode on the reactant side of the MEP. This change is not compensated for by a

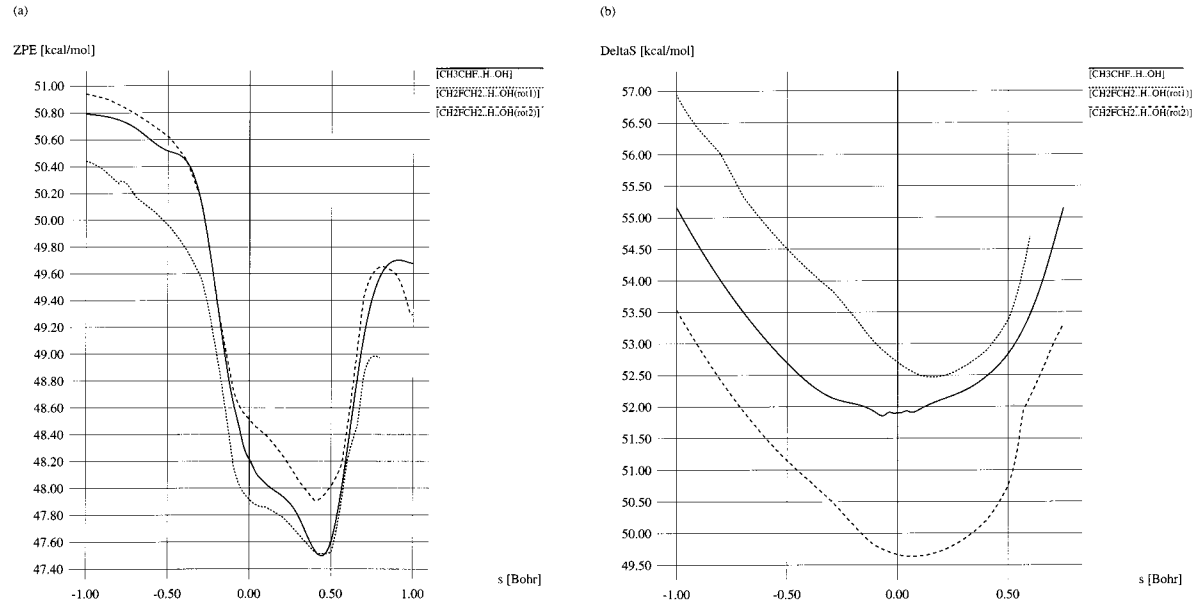

Figure 4. (a) The zero-point energy and (b) the entropy change along the reaction path for reactions R_F1, R_F2a, and R_F2b.

lowering of the potential energy since the reaction path is relatively flat in this region. On the product side, the MEP is much steeper and the change in potential energy along the reaction path is greater than is the change in the zero-point energy. For the R_F2b reaction the reactant side of the MEP is already steep enough to compensate for vibational changes resulting in a negligible variational effect. Adding in entropic effects shifts the dynamic bottleneck slightly in the product direction for all three reactions, resulting in $s_*^{AG} = -0.2708a_0$ for R_F2a and $s_*^{AG} = -0.0018a_0$ for R_F2b, again in comparison to $s_*^{AG} = -0.3255a_0$ for R_F1. This illustrates the competition between the potential energy, the vibrational energy and the entropy in determining the location of the variational transition state. Figure 3 shows the Born−Oppenheimer energy along the minimum energy path ($V_{MEP}(s)$), the vibrationally adiabatic ground-state potential energy curve ($V_a^G(s)$), and the free energy curve for the reactions R_F1, R_F2a, and R_F2b. It is interesting to note that vibrational and entropic effects lessen the differences between the two reaction pathways for hydrogen atom abstraction from the primary carbon thus diminishing the energy preference of the [$CH_3CHF\cdots H\cdots OH$(rot2)] transition-state structure gained through the weak interactions between the halogen and the hydrogen of the OH radical. This can be further demonstrated by plotting changes in the zero-point energies and entropy contributions as a function of the reaction coordinate as shown in Figure 4. The strongest H−F interaction in the [$CH_3CHF\cdots H\cdots OH$(rot2)] structure results in stiffer small vibrational frequencies which leads to the smaller entropy correction. The reaction rate constants calculated at 298.15 K are $5.31 \times \mathbf{10}^{-15}$ cm^3/molecule s for R_F1, $8.54 \times \mathbf{10}^{-16}$ cm^3/molecules for R_F2a and $1.40 \times \mathbf{10}^{-15}$ cm^3/molecule s for R_F2b. Accounting for tunneling effects, via the small curvature tunneling approximation, increases the reaction rate constants by a factor of 3.9 for R_F2a and 3.6 for R_F2b, in comparison to 3.5 for R_F1 at 298.15 K. This yields an overall reaction rate constant of $2.69 \times \mathbf{10}^{-14}$ cm^3/molecule s in comparison with the experimental value[43] of $2.13 \times \mathbf{10}^{-13}$ cm^3/molecule s. Discrepancies between calculated and experimental results have already been discussed in previous papers; e.g., ref 8e and f. The change in the contribution of each reaction pathway to the overall reaction rate as a function of temperature is given in Figure 5a. For reaction R_F2a the contribution to the overall reaction rate increases with increasing temperature, while for the R_F1 and R_F2b reaction pathways the opposite trend is observed.

Excitation of Reactive Vibrational Modes. It has been noted[8e] that on the basis of vibrational-mode correlation analysis, and on calculated nonadiabatic coupling constants, the excitation of the ν(OH), $\nu(CH_2)$, and $\delta(CH_2)$ vibrational modes can significantly increase the abstraction rate for the R_F1 reaction. In this work the statistical vibrationally diabatic model was employed to calculate vibrational-state selected rate constants for the reactions R_H1, $R_{Cl}1$, R_F1, R_F2a, and R_F2b. (The temperature dependence of the vibrational enhancement factors for exciting modes ν(OH), $\nu(CH_2)$, and $\delta(CH_2)$ into their first excited state are given in Table 2.) An increase in the reaction rate is predicted for exciting any of these three modes. Significant enhancements in the rate constants are predicted for the excitation of the $\nu(CH_2)$ mode for all reactions studied in this work, while excitation of the ν(OH) mode has a negligible effect on the computed reaction rate. Excitation of the $\delta(CH_2)$ mode increases the reaction rates by approximately 20%−50%. An inverse correlation between temperature and enhancement factors is observed. At 298 K the difference between thermal and state-selected reaction rates is a factor of 6 for the R_H1 reaction, a factor 9 for the $R_{Cl}1$ reaction, a factor 6 for the R_F1 reaction, a factor 11 for the R_F2a reaction and a factor 15 for the R_F2b reaction. It is interesting to note that the excitation of the C−H stretching mode leads to a significantly greater enhancement factor for the R_F2b reaction than it does for the R_F1 reaction. Therefore, vibrational excitation is predicted to have a greater effect on primary abstraction than on secondary abstraction. The change in the contribution by each reaction pathway to the overall reaction rate (with the $\delta(CH_2)$ mode excited) as a function of temperature is presented in Figure 5b. From Figure 5b a significant increase in the R_F2a contribution to the overall reaction rate is predicted, leading to equal contributions by the R_F2a and R_F2b reaction pathways at temperatures higher that 400 K in comparison to 10% and 40% respectively at 250 K. The position of the dynamical bottleneck is greatly influenced by the excitation of $\delta(CH_2)$. (The variational shifts with respect to the ground-state vibrational energy curve maxima are given in Table 3.) Excellent correspondence between room-temperature dynamical-bottleneck locations and

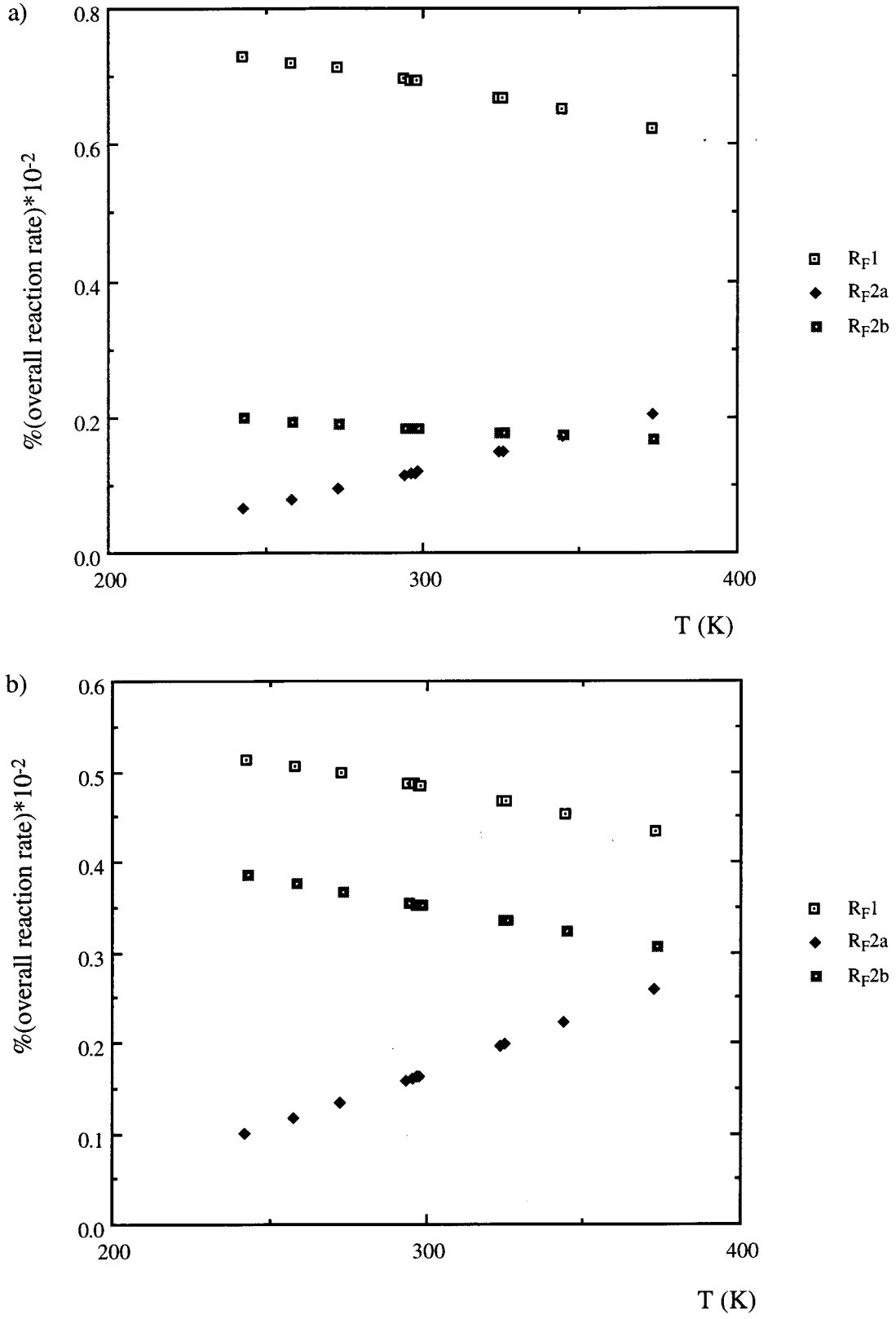

Figure 5. The change in the contribution of the R_F1, R_F2a, and R_F2b reaction pathways to the overall reaction rate for (a) the vibrational ground state and (b) the vibrationally excited-state as a function of temperature.

diabatic-curve-potential maxima are observed with a shift toward the saddle point as the temperature is raised.

Features of the PM3-SRP Potential Energy Function. Both the standard PM3 parameters and our optimized specific reaction parameters are presented in Table 4. The largest differences between the parameter sets are found for $U_{ss}^{(o)}$, $U_{ss}^{(CH)}$, and $\beta_P^{(o)}$. It seems "chemically" reasonable that the barrier height for the abstraction reaction (where the new bond is formed between the leaving hydrogen and the oxygen of the hydroxyl radical) would be sensitive to the value of $U_{ss}^{(o)}$, and to the core resonance integrals β, which describe the major contribution to the bonding interaction between two atoms.[18c]

TABLE 2: Temperature Dependence of the Vibrational Enhancement Factors for the Reactions R_H, R_F, and R_{Cl} with ν(OH), $\nu(CH_2)$, and $\delta(CH_2)$ in Their First Excited State: These Rate Constants Were Calculated at the (G2//MP2)/SCT Level

	[$CH_3CFH\cdots H\cdots OH$]			[$CH_2FCH_2\cdots H\cdots OH$(rot1)]			[$CH_2FCH_2\cdots H\cdots OH$(rot2)]		
T (K)	ν(OH)	$\delta(CH_2)$	$\nu(CH_2)$	ν(OH)	$\delta(CH_2)$	$\nu(CH_2)$	ν(OH)	$\delta(CH_2)$	$\nu(CH_2)$
243	1.09	1.01	7.49	1.08	1.24	15.28	1.20	1.36	20.36
273	1.08	1.01	6.40	1.07	1.24	12.61	1.17	1.31	17.45
298	1.07	1.01	5.70	1.07	1.24	10.92	1.16	1.28	15.45
325	1.07	1.01	5.10	1.06	1.23	9.52	1.14	1.25	13.66
373	1.06	1.01	4.32	1.05	1.22	7.78	1.12	1.20	11.23

	[$CH_3CH_2\cdots H\cdots OH$]			[$CH_3CClH\cdots H\cdots OH$]			
T (K)	ν(OH)	$\delta(CH_2)$	$\nu(CH_2)$	T (K)	ν(OH)	$\delta(CH_2)$	$\nu(CH_2)$
248	1.05	1.57	7.35	250	1.12	1.26	10.22
273	1.05	1.52	6.73	270	1.11	1.23	8.85
297	1.05	1.48	6.23	298	1.11	1.24	9.03
340	1.04	1.41	5.48	330	1.09	1.18	5.17
374	1.04	1.38	5.03	381	1.08	1.17	4.57
395	1.04	1.37	4.81	421	1.07	1.16	4.26
427	1.04	1.34	4.49	490	1.06	1.13	3.43
462	1.04	1.33	4.22	548	1.05	1.12	3.17
483	1.03	1.30	4.03	595	1.05	1.11	3.14
578	1.01	1.24	3.45	600	1.05	1.11	2.96
704	1.02	1.21	2.99	788	1.04	1.08	2.49

TABLE 3: VTST Bottleneck Location at 298 K

	$s^*(n_{\nu(OH)}, n_{\nu(CH_2)}, n_{\delta(CH_2)})/a_0$				
	R_H1	$R_{Cl}1$	R_F1	R_F2a	R_F2b
(0,0,0)	−0.2581	−0.2708	−0.3112	−0.2707	−0.0018
(1,0,0)	−0.2579	−0.2670	−0.3063	−0.2698	−0.0013
(0,1,0)	−0.4157	−0.5360	−0.3887	−0.5017	−0.0546
(0,0,1)	−0.3046	−0.2767	−0.2939	−0.2787	−0.4015

TABLE 4: Optimized PM3 Specific Reaction Parameters

parameter	atom	PM3	PM3-SRP	Δ
U_{ss}	H	−13.073 321	−14.588 627	1.52
G_{ss}	H	14.794 208	15.361 569	−0.57
β_s	H	−5.626 512	−6.195 294	0.57
U_{ss}	C	−47.270 320	−46.944 706	−0.33
U_{pp}	C	−36.266 918	−37.425 882	1.16
G_{ss}	C	11.200 708	10.656 471	0.54
G_{sp}	C	10.265 027	9.703 922	0.56
G_{pp}	C	10.796 292	10.607 843	0.19
G_{p2}	C	9.042 566	9.413 725	−0.37
H_{sp}	C	2.290 980	2.357 059	−0.07
β_s	C	−11.910 015	−12.045 882	0.14
β_p	C	−9.802 755	−9.806 118	0.00
U_{ss}	O	−86.993 002	−95.700 000	8.71
U_{pp}	O	−71.879 580	−71.971 765	0.09
G_{ss}	O	15.755 760	16.010 588	−0.25
G_{sp}	O	10.621 160	10.115 686	0.51
G_{pp}	O	13.654 016	13.525 882	0.13
G_{p2}	O	12.406 095	12.487 059	−0.08
H_{sp}	O	0.593 883	0.578 824	0.02
β_s	O	−45.202 651	−45.123 529	−0.08
β_p	O	−24.752 515	−27.323 529	2.57

[a] U, the one-center electron kinetic energy and nuclear attraction in eV; G and H, the two-electron one-center repulsion integrals in eV; β, the resonance integral in eV. Indices correspond to the atomic basis.

The important geometric parameters, investigated at both the ab initio and the semiempirical levels of theory, are reported in Table 5. It is interesting to note that barriers calculated with the standard PM3 Hamiltonian are not as greatly overestimated for our reactions as they are for some other H transfer reactions;[20] however, the reaction enthalpies and the imaginary frequencies are greatly overestimated. Thus, reparametrization of the PM3 Hamiltonian leads to a far more reliable potential energy surface than would otherwise be obtained with the standard parametrization. Reparametrization did not improve, significantly, the breaking and forming bond lengths although both the PM3 and the PM3-SRP geometries more closely resemble those obtained at the MP2 level of theory than do those computed at the Hartree−Fock[8a,8b] level.

For all six reactions very good results were obtained using the PM3-SRP parameters that were optimized to describe the ethane reaction. Such results are very encouraging in that they show, at least for this case, the specific reaction parameters are general for reactions of the same mechanism. The minimum energy path for the ethane reaction with the OH radical, computed at several different levels of theory, is given in Figure 6.

As an experiment we took five generic hydrocarbons for which the abstraction rates are reported in ref 3b and applied the direct NDDO−SRP/μOMT method described above. Such systems are representative of the hydrocarbons which are important in atmospheric and combustion chemistry. We report the results in Table 6. The reported rates are sums of the individual rates for each of the several abstraction pathways we found with no attempt to weight the individual contributions. The results reported in Table 6 are encouraging, but further investigations are both needed and ongoing.

It should be noted that the PM3-SRP method overestimates hydrogen−hydrogen interactions. (This is true for the original PM3 parametrization also.) Because of this, transition-state conformers studied in this work involving O−H rotations are too strongly hindered. We corrected for this behavior through Interpolated corrections. That is, by fitting the hindered rotation (with this "spurious" H−H interaction) to a hindered O−H rotation without this overestimation.

The temperature dependence of the reaction rate constants calculated at the (G2//MP2)/SCT, (G2/MP2///SRP)/μOMT, and SRP/μOMT levels for the ethane, fluoroethane, and chloroethane reactions are given in Figure 7. For the halogenated ethanes the overall reaction rates are reported as the sum of the R_x1 and the R_x2 reaction pathways. The only exception is the (G2//MP2)/SCT rate constant for the chloroethane reaction. The ab initio reaction path data were only available for the $R_{Cl}1$ reaction; thus, the reported rate should be approximately 80% of the overall reaction rate. It should be stressed here that the (G2//MP2)/SCT rate constants given in Figure 7 differ from those published previously[8e] due to the differences in the range

TABLE 5. Barrier Heights, Reaction Enthalpies, Reactive Bond Lengths, and Imaginary Vibrational Frequencies Calculated at the ab Initio and Semiempirical Levels of Theory for the Reactions R_H1, R_F1, R_F2a, R_F2b, $R_{Cl}1$, $R_{Cl}2a$, and $R_{Cl}2b$

	[CH_3CH_2···H···OH]					[CH_3CFH···H···OH]				
method	$\Delta E^{\ddagger}$	$\Delta_r H$	r_{CH}	r_{OH}	ν_i	$\Delta E^{\ddagger}$	$\Delta_r H$	r_{CH}	r_{OH}	ν_i
MP2/6-31G(d,p)	5.5	−14.3	1.107	1.321	1775	3.9	−16.9	1.191	1.314	1920
G2(MP2)	2.9	−17.7				2.0	−18.4			
PM3	7.9	−26.7	1.229	1.337	2484	6.2	−30.5	1.239	1.359	2552
SRP[a]	3.8	−19.3	1.219	1.336	2267	2.2	−19.3	1.225	1.371	2349
	[CH_2FCH_2···H···OH(rot1)]					[CH_2FCH_2···H···OH(rot2)]				
method	$\Delta E^{\ddagger}$	$\Delta_r H$	r_{CH}	r_{OH}	ν_i	$\Delta E^{\ddagger}$	$\Delta_r H$	r_{CH}	r_{OH}	ν_i
MP2/6-31G(d,p)	6.5	−11.7	1.200	1.292	1951	4.0	−11.7	1.210	1.273	2108
G2(MP2)	3.3	−14.9				4.3	−14.9			
PM3	9.8	−23.9	1.226	1.314	2489	8.8	−23.9	1.226	1.321	2464
SRP[a]	5.3	−14.1	1.217	1.316	2273	4.9	−14.1	1.217	1.325	2276
	[CH_3CClH···H···OH]					[CH_2ClCH_2···H···OH(rot1)]				
method	$\Delta E^{\ddagger}$	$\Delta_r H$	r_{CH}	r_{OH}	ν_i	$\Delta E^{\ddagger}$	$\Delta_r H$	r_{CH}	r_{OH}	ν_i
MP2/6-31G(d,p)	4.1	−17.6	1.187	1.313	1957	5.8	−13.6	1.196	1.302	1907
G2(MP2)	1.1	−21.3				3.4	−16.9			
PM3	7.3	−30.9	1.243	1.357	2595	9.0	−24.6	1.229	1.326	2517
SRP[a]	2.0	−16.22	1.234	1.390	2353	4.9	−16.9	1.183	1.395	2285

	[CH_2ClCH_2···H···OH(rot2)]				
method	$\Delta E^{\ddagger}$	$\Delta_r H$	r_{CH}	r_{OH}	ν_i
MP2/6-31G(d,p)	4.9	13.6	1.204	1.281	2054
G2(MP2)	2.8	−16.9			
PM3	8.4	−24.6	1.230	1.325	2498
SRP[a]	4.3	−16.9	1.220	1.330	2294

[a] The SRP were obtained for the ethane reaction with OH radical at G2(MP2)///PM3-SRP.

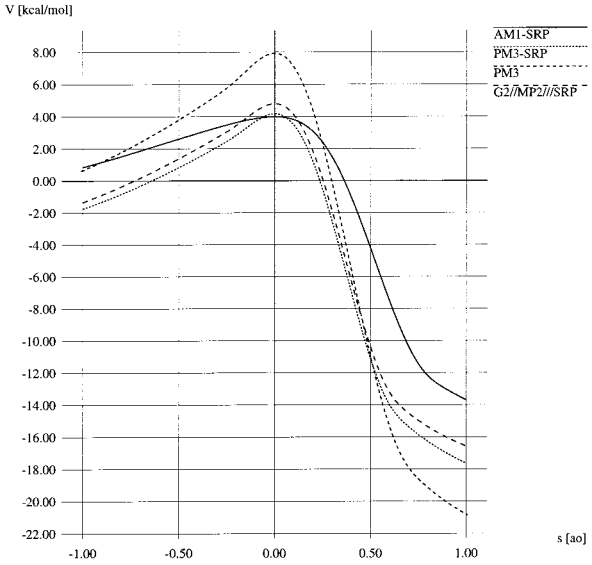

Figure 6. The Born−Oppenheimer potential energy (V_{MEP}) for the ethane reaction with the OH radical calculated at various levels of theory.

parameter L. In this work larger values of L were used since they were fitted with respect to the energies of the prereaction complexes. As a result, the thickness of the fitted potential energy curves were reduced and the tunneling corrections increased. The room-temperature rate constant for the R_H, R_F, and R_{Cl} reactions are respectively 24%, 55%, and 33% higher than the rate constants published previously.[8e] It is interesting to note that the increases in the computed reaction rate constants correlate with the stabilization energy of the corresponding prereactive complexes; i.e., −0.2, −2.7, and −2.3 kcal/mol for reactions R_H, R_F, and R_{Cl} respectively.[8f]

An approximate least-imaginary-action principle is used to select the tunneling method that gives the largest tunneling probabilities.[46] On the PM3-SRP potential energy surfaces large-curvature tunneling is the dominant tunneling pathway for reactions R_H, R_F2a, R_F2b, $R_{Cl}2a$, and $R_{Cl}2b$. For reactions R_F1 and $R_{Cl}1$, the small-curvature approximation leads to larger tunneling probabilities due to the lower barrier heights. When interpolated corrections were applied, all barrier heights are further decreased and small-curvature tunneling becomes the dominant tunneling pathway.

Figure 7a illustrates very dramatically that the widely discussed curvature of the Arrhenius plot of the ethane reaction is almost entirely due to tunneling. Thus the CVT calculation at the (G2//MP2)/SCT level plots out as nearly a straight line, while the nonlinear (G2/MP2///SRP)/μOMT curve tracks the experimental results rather faithfully. The average difference between the experimental and the calculated reaction rates for the ethane reaction is lowered from a factor of 5.3 to factor of 1.1 for (G2//MP2)/SCT vs (G2/MP2///SRP)/μOMT calculations. For fluoroethane this lowering is even larger going from 10.7 to 2.1. The situation for chloroethane is comparable, 13.2 to 2.5, but the exact values cannot be obtained since the (G2//MP2)/SCT rate constants were calculated for the secondary abstraction only.

For the ethane reaction the SRP/μOMT and (G2/MP2///SRP)/μOMT rate constants are almost the same, with the (G2/MP2///SRP)/μOMT rate constants being a factor of 0.860 smaller (a factor of 1.47 smaller using the LCT correction). In the cases of fluoroethane and chloroethane the differences between the SRP/μOMT and (G2/MP2///SRP)/μOMT rate constants are somewhat larger, with the experimental values laying approximately between, see Figure 7. The (G2/MP2///SRP)/μOMT rate constants are factors of 0.223 (0.228 for the LCT correction) and 0.256 (0.395 for the LCT correction) lower than are the

TABLE 6: Example GRP (Ethane) Abstraction Results: Cited Experimental Rates from Reference 3b and All Reported Rates Multiplied by 10^{12}

	n-butane (C_4H_{10})		*n*-pentane (C_5H_{12})		2,2-dimethylpropane(C_5H_{12})	
	$k^{298}_{CVT/\mu OMT}$	$k^{298}_{CVT/LCT}$	$k^{298}_{CVT/\mu OMT}$	$k^{298}_{CVT/LCT}$	$k^{298}_{CVT/\mu OMT}$	$k^{298}_{CVT/LCT}$
Ts1	2.79	1.40	0.30	0.15	1.03	0.73
Ts2	9.71	5.41	0.27	0.27		
Ts3	0.69	0.69	1.17	1.13		
Ts4			1.07	1.03		
sum	1.07	0.87	2.81	2.58	1.03	0.73
corr[a]	0.92	1.22	2.42	3.79	0.89	1.07
exptl	1.68−4.2		4.01−6.60		0.50−2.00	

	2,2-dimethylhexane		octane	
	$k^{298}_{CVT/\mu OMT}$	$k^{298}_{CVT/LCT}$	$k^{298}_{CVT/\mu OMT}$	$k^{298}_{CVT/LCT}$
Ts1	0.02	0.01	0.24	0.12
Ts2	0.05	0.03	0.20	0.13
Ts3	1.49	1.88	0.99	0.97
Ts4	2.23	1.19	1.60	1.68
Ts5	2.10	0.94	1.47	1.44
Ts6	0.01	0.01		
Ts7	0.04	0.01		
Ts8	0.08	0.07		
Ts9	0.01	0.01		
Ts10	0.02	0.02		
sum	6.05	4.17	4.50	4.34
corr[a]	5.20	6.12	3.87	6.38
exptl	4.79−4.87		7.17−9.67	

[a] Correction factor for the $k^{298}_{CVT/\mu OMT}$ is 0.86 and for $k^{298}_{CVT/LCT}$ 1.47

SRP/μOMT values for the fluoroethane and chloroethane reactions, respectively. These differences are almost constant within the investigated temperature range for the SRP//μOMT rate constants. Therefore, they can be used as correction factors for the *low-level* rate constants calculated for the larger systems of interest.

The temperature dependence of the (G2/MP2///SRP)/LCT and SRP/LCT ratios is somewhat stronger; therefore, the factors given in parentheses are the averages over the 200−400 K temperature range. It is interesting to note that the experimental rate constants fall between the (G2/MP2///SRP)/μOMT and SRP/μOMT results implying that, possibly, these two methods can be used as bounds in predicting the rate constants of species for which the experimental values are not available.

Conclusions

The results reported in this study were based on high-level electronic structure calculations, interpolated variational transition state theory, and dual-level direct dynamics calculations with multidimensional semiclassical tunneling corrections. Reaction rate constants for primary abstraction from fluoroethane were calculated in terms of interpolated variational transition state theory at the (G2//MP2)/SCT level of theory and compared with previously calculated rate constants for abstraction from the secondary carbon atom. This to study the relationship between energetic and entropic effects in the determination of the dynamical bottleneck. It was found that both vibrational and entropic effects minimize the differences between the two different primary carbon abstraction reaction pathways, thus diminishing the energy preference of the [CH_3-CHF···H···OH(rot2)] transition-state structure gained through weak interactions between the halogen atom and the hydroxyl hydrogen. Abstraction of hydrogen from the secondary carbon atom was found to contribute 80% to the overall rate, and the ratio diminishes with increasing temperature.

The statistical diabatic model was used to provide qualitative analysis on the possible vibrational-state specific chemistry of these hydrogen abstraction reactions. Significant enhancements of the rates are predicted for the excitation of the $\delta(CH_2)$ mode of the reactant hydrocarbon molecule. An inverse correlation between the absolute temperature and the enhancement factors was found.

To obtain useful semiempirical potential energy surfaces for the studied reactions a set of specific reaction parameters was obtained by re-parametrizing the semiempirical PM3 Hamiltonian. Rates obtained via the use of these specific reaction parameters (obtained for the ethane reaction) were compared to those determined via the G2(MP2)//MP2/6-31G(d,p) approach for both ethane and fluoroethane. Very good agreement was found not only for the ethane reaction (for which the PM3 Hamiltonian was reparametrized) but also for the fluoroethane reaction as well. Ab initio results for abstraction from the secondary carbon atom in chloroethane are surprisingly well reproduced through the use of the PM3-SRP Hamiltonian. Further, the PM3-SRP approach was used to study abstraction from the primary carbon of chloroethane. Our findings give us confidence that the SRPs are not "strictly" reaction specific but that they can be used for other reactions of the same mechanism type. (See Table 6.) If this is generally so, reaction rates of larger hydrocarbons (of interest in atmospheric and combustion chemistry) may then be predicted both reliably and at low computational cost.

Multidimensional tunneling calculations were carried out in the small-curvature, large-curvature, and microcanonical optimized multidimensional tunneling approximations. For the PM3-SRP potential energy surfaces large-curvature tunneling was found to be the dominant tunneling pathway for most of the reactions studied. For reactions R_F1 and $R_{Cl}1$ the small-curvature approximation led to larger tunneling probabilities due to lower barrier heights. When interpolated corrections were applied all barrier heights were further decreased and small-curvature tunneling became the dominant tunneling pathway.

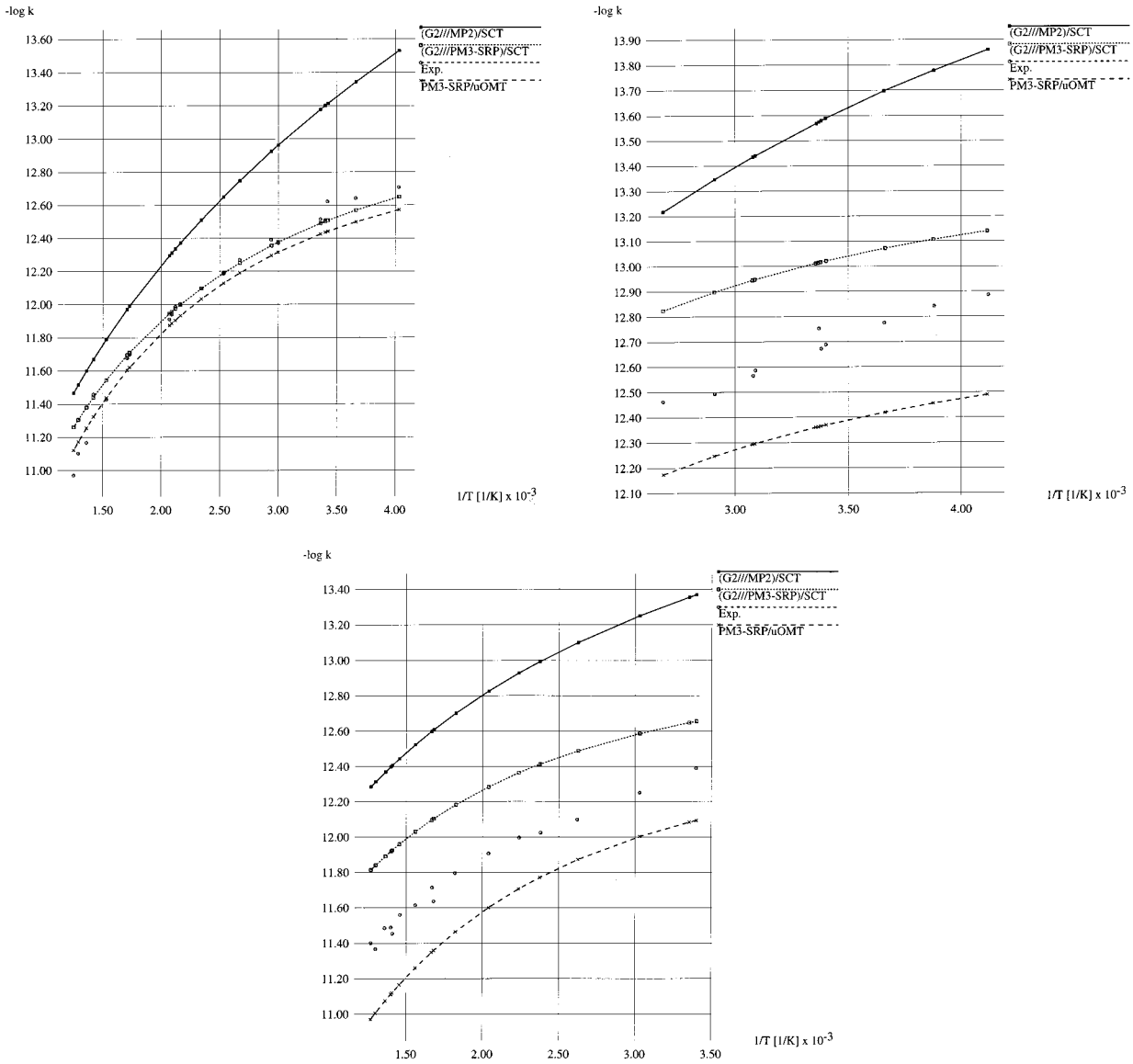

Figure 7. The temperature dependence of the experimental, and the calculated, reaction rate constants for the (a) ethane, (b) fluoroethane, and (c) chloroethane reactions with the hydroxyl radical.

The temperature dependence of the rate constants calculated at the (G2/MP2///SRP)/μOMT level of theory were compared to those of experiment. Our computed reaction rates for ethane are within the range of 0.9−1.9 of the experimental result for the 250−800 K temperature range. For fluoroethane and chloroethane these factors are somewhat higher, but still very satisfactory, with average values of 2.1 and 2.5, respectively. (For R_H, R_{Cl}, and R_F over the temperature range of 200−400 K the average correction factors were found to be, respectively, 3.5, 2.0, and 11.5.

For molecular systems which are much larger than these, ab initio corrections to the NDDO-SRP surface will become too computationally demanding to be generally useful. Thus we sought an alternative in the form of correction factors to the inexpensive NDDO-SRP result. We define these correction factors to be the ratios of the (G2/MP2///SRP)/μOMT and NDDO−SRP/μOMT rate constants. These ratios may prove useful in improving the low level NDDO-SRP/μOMT computed rates such that they become a good approximation to those obtained via the higher level (G2/MP2///SRP)/μOMT method, over a range of temperatures, for larger molecular systems reacting via the same mechanism.

Acknowledgment. This work was supported by the AFOSR under Grant F49620-98-0116, by Grant P00890605 awarded by the Ministry of Science and Technology of the Republic of Croatia, and by the U.S.−Croatian Science and Technology Joint Fund in cooperation with U.S. Department of Agriculture and Croatian Ministry of Science and Technology under Project Number JF-120. This work was also carried out under the framework of the project "Fate and Activity Modeling of Environmental Pollutants using Structureactivity Relationships (FAME)", financially supported by the Environment and Climate Research and Technological Development Program of the Commission of the European Union under Contract ENV4-CT96-0211 (DG 12-ESCY). Financial support from the European Union is gratefully acknowledged.

References and Notes

(1) Barker, J. R., Ed. *Progress and Problems in Atmospheric Chemistry*, Advanced Series in Physical Chemistry 3; World Scientific Publishing Co.: Singapore, 1995.

(2) (a) Manzer, L. *Science* **1990**, *249*, 31. (b) Solomon, S. *Nature* **1990**, *347*, 6291. (c) Freemantle, M. *Chem. Eng. News* **1994**, *72*, 2. (d) Schwarzbach, S. E. *Nature* **1995**, *376*, 297.

(3) (a) Atkinson, R. *Chem. Rev.* **1986**, *86*, 69. (b) Atkinson, R. *J. Phys. Chem. Ref. Data Monogr.* **1989**, 1. (c) Atkinson, R.; Baulch, D. L.; Cox,

R. A.; Hampson, R. F. Jr.; Kerr, J. A.; Troe, J. *J. Phys. Chem. Ref. Data* **1989**, *18*, 881. (d) Atkinson, R. *J. Phys. Chem. Ref. Data*, **1994**, *2*.

(4) (a) Stolarski, R.; Bojkov, R.; Bishop, L.; Zerefos, C.; Staehelin, J.; Zawodny, J. *Science* **1992**, 256, 342. (b) Kerr, R. A. *Science* **1993**, 262, 501. (c) Kerr, J. B.; McElroy, C. T. *Science* **1993**, *262*, 1032. (d) Newman, A. *Environ. Sci. Technol.* **1993**, *27*, 1488. (e) Ravishankara, A. R.; Turnipseed, A. A.; Jensen, N. R.; Barone, S.; Mills, M.; Howard, C. J.; Solomon, S. *Science* **1994**, *263*, 71. (f) Schwarzbach, S. E. *Nature* **1995**, 376, 297.

(5) (a) Dorigo A. E.; Houk, K. N. *J. Org. Chem.* **1988**, *53*, 1650. (b) Truong, T. N.; Truhlar, D. G. *J. Chem. Phys.* **1990**, *93*, 1761. (c) Gonzales, C.; McDouall, J. J. W.; Schlegel, H. B. *J. Phys. Chem.* **1990**, *94*, 7467. (d) Lasaga, A. C.; Gibbs, G. V. *Geophys. Res. Lett.* **1991**, *18*, 1217. (e) Dobbs, K. D.; Dixon, D. A.; Komornicki, A. *J. Chem. Phys.* **1993**, *98*, 8852. (f) Francisco, J. S. *J. Chem. Phys.* **1992**, *96*, 7597. (g) Francisco, J. S. *J. Chem. Soc., Faraday Trans.* **1992**, *88*, 1943. (h) McKee, M. L. *J. Phys. Chem.* **1993**, *97*, 10971. (i) Rayez, M.-T.; Rayez, J.-C.; Berces, T.; Lendvay, G. *J. Phys. Chem.* **1993**, *97*, 5570. (j) Bottoni, A.; Poggi, G.; Emmi, S. S. *J. Mol. Struct. (THEOCHEM)* **1993**, 279, 229. (k) Walch, S. P. *J. Chem. Phys.* **1993**, *98*, 3163. (m) Fu, Y. J.; Lewisbevan, W.; Tirrell J. *J. Phys. Chem.* **1995**, *99*, 630.

(6) (a) Melissas, V. S.; Truhlar, D. G. *J. Chem. Phys.* **1993**, 98, 1013. (b) Melissas, V. S.; Truhlar D. G. *J. Chem. Phys.* **1993**, *99*, 3542. (c) Melissas, V. S.; Truhlar, D. G. *J. Phys. Chem.* **1994**, *98*, 875. (d) Corchado, J. C.; Espinosa-Garcia, J.; Hu, W.-P.; Rossi, I.; Truhlar, D. G. *J. Phys. Chem.* **1995**, *99*, 687. (e) Hu, W.-P.; Rossi, I.; Corchado, J. C.; Truhlar, D. G. *J. Phys. Chem.* A **1997**, *101*, 6911.

(7) (a) Martell, J. M.; Mehta, A. K.; Pacey, P. D.; Boyd, R. J. *J. Phys. Chem.* **1995**, *99*, 8661. (b) Martell, J. M.; Boyd, R. J. *J. Phys. Chem.* **1995**, *99*, 13402.

(8) (a) Sekušak, S.; Güsten, H.; Sabljić, A. *J. Chem. Phys.* **1995**, *102*, 7504. (b) Sekušak, S.; Güsten, H.; Sabljić, A. *J. Phys. Chem.* **1996**, *100*, 6212. (c) Sekušak, S.; Güsten, H.; Sabljić, A. *J. Phys. Chem. A* **1997**, 101, 967 (correction). (d) Sekušak, S.; Sabljić, A. *J. Comput. Chem.* **1997**, 18, 1190. (e) Sekušak, S.; Liedl, K. R.; Rode, B. M.; Sabljić, A. *J. Phys. Chem. A* **1997**, *101*, 4245. (f) Sekušak, S.; Sabljić, A. *Chem. Phys. Lett.* **1997**, *272*, 353.

(9) Truhlar, D. G. In *The Reaction Path in Chemistry: Current Approaches and Perspectives*; Heidrich, D., Ed.; Kluwer: Dordrecht, 1995; p 229.

(10) Truhlar, D. G.; Garrett, B. C. *Acc. Chem. Res.* **1980**, *13*, 440.

(11) Truhlar, D. G.; Isaacson, A. D.; Garrett, B. C. In *Theory of Chemical Reaction Dynamics*; Baer, M., Ed.; CRC Press: Boca Raton, 1985; Vol. 4, p 65.

(12) (a) Liu, Y.-P.; Lynch, G. C.; Truong, T. N.; Lu, D.-h.; Truhlar, D. G.; Garrett, B. C. *J. Am. Chem. Soc.* **1993**, *115*, 2408.

(13) (a) Truhlar, D. G.; Isaacson, A. D.; Skodje, R. T.; Garrett, B. C. *J. Phys. Chem.* **1982**, *86*, 2252. (b) Truhlar, D. G.; Isaacson, A. D.; Skodje, R. T.; Garrett, B. C. *J. Phys. Chem.* **1982**, *86*, 2252.

(14) Garett, B. C.; Joseph, T.; Truong, T. N.; Truhlar, D. G. *Chem. Phys.* **1989**, *136*, 271.

(15) (a) Benderskii, V. A.; Marakov, D. E., Wight, C. A. *Chemical Dynamics at Low Temperatures*; Prigogine, I., Rice, S. A, Eds.; John Wiley: NY, 1994.

(16) Garrett, B. C.; Truhlar, D. J. *J. Am. Chem. Soc.* **1979**, *101*, 4534. (b) Garrett, B. C.; Truhlar, D. J. *J. Am. Chem. Soc.* **1979**, *101*, 5207.

(17) (a) Hu, W.-P.; Liu, Y.-P.; Truhlar, D. G. *J. Chem. Soc., Faraday. Trans.* **1994**, *90*, 1715. (b) Corchado, J. C.; Espinosa-Garcia, J.; Hu, W.-P.; Rossi, I.; Truhlar, D. G.; *J. Phys. Chem.* **1995**, *99*, 4618.

(18) (a) Stewart, J. J. P. *J. Comput. Chem.* **1989**, *10*, 209. (b) Stewart, J. J. P. *Comput.-Aided Mol. Des.* **1990**, *4*, 48. (c) Dewar, M. J.; Thiel, W. *J. Am. Chem. Soc.* **1977**, *99*, 4899, 4907.

(19) (a) Rossi, I.; Truhlar, D. G. *Chem. Phys. Lett.* **1995**, *233*, 231−236. (b) Gonzalez-Lafont, A.; Truong, T. N.; Truhlar, D. G. *J. Phys. Chem.* **1991**, *95*, 4618.

(20) (a) Kim, Y. *J. Am. Chem. Soc.* **1996**, *118*, 1522. (b) Loerting, T.; Liedl, K. R.; Rode, B. M. *J. Am. Chem. Soc.* **1980**, *102*, 404.

(21) (a) Bartlett, R. J. *Annu. Rev. of Phys.* **1981**, *32*, 359. (b) Bartlett, R. J. *J. Phys. Chem.* **1989**, *93*, 1697.

(22) Hariharan, P. C.; Pople, J. A *Chem. Phys. Lett.* **1972**, *66*, 217.

(23) Gonzalez, C.; Schlegel, H. B *J. Phys. Chem.* **1990**, *94*, 5523.

(24) Miller, W. H.; Handy, N. C.; Adams, J. E. *J. Chem. Phys.* **1980**, *72*, 99.

(25) Schlegel, H. B. *J. Phys. Chem.* **1988**, *92*, 3075.

(26) (a) Curtiss, L. A.; Raghavachari, K.; Pople, J. A. *J. Chem. Phys.* **1993**, *98*, 1293. (b) Pople, J. A.; Head-Gordon, M.; Fox, D. J.; Raghavachari, K.; Curtiss, L. A. *J. Chem. Phys.* **1989**, *90*, 5622. (c) Curtiss, L. A.; Raghavachari, K.; Trucks, G. W.; Pople, J. A. *J. Chem. Phys.* **1991**, *94*, 7221.

(27) Stewart, J. J. P.; Rossi, I.; Hu, W.-P.; Lynch, G. C.; Liu, Y.-P.; Truhlar, D. G. MOPAC Version 5.05mn; University of Minnesota; Minneapolis, 1995.

(28) (a) Frisch, A. M. J.; Trucks, G. W.; Head-Gordon, M.; Gill, P. M. W.; Wong, M. W.; Foresman, J. B.; Johnson, G. B.; Schlegel, H. B.; Robb, M. A.; Replogle, E. S.; Gomperts, R.; Anders, J. L.; Raghavachari, K.; Binkley, J. S.; Gonzalez, C.; Martin, R. L.; Fox, D. J.; Defrees, D. J.; Baker, J.; Stewart, J. J. P.; Pople, J. A. *Gaussian92*; Gaussian, Inc.; Pittsburgh, PA, 1992. (b) Frisch, A. M. J.; Trucks, G. W.; Schlegel, H. B.; Gill, P. M. W.; Johnson, B. G.; Robb, M. A.; Cheesman, J. R.; Keith, T. A.; Petersson, G. A.; Montgomery, J. A.; Raghavachari, K.; Al-Laham, M. A.; Zakrzewski, V. G.; Ortiz, J. V.; Foresman, J. B.; Cioslowski, J.; Stefanov, B. B.; Nanayakkara, A.; Challacombe, M.; Peng, C. Y.; Ayala, P. Y.; Chen, W.; Wong, M. W.; Andres, J. L.; Replogle, E. S.; Gomperts, R.; Martin, R. L.; Fox, D. J.; Binkley, J. S.; Defrees, D. J.; Baker, J.; Stewart, J. P.; Head-Gordon, M.; Gonzalez, C.; Pople, J. A. *Gaussian 94*, Revision C.2; Gaussian, Inc.: Pittsburgh, PA, 1995.

(29) Carroll, D. L. *GaFortran*, Version 1.6.4; University of Illinois: Champaign-Urbana, 1997.

(30) Goldberg, D. E. *Genetic Algorithms in Search, Optimization and Machine Learning. Physical Chemistry*. Addison-Wesley: Reading, MA, 1989.

(31) Liu, Y.-P.; Lu, D.-h.; Gonzalez-Lafont, A.; Truhlar, D.; Garrett, B. C. *J. Am. Chem. Soc.* **1993**, *115*, 7806.

(32) (a) Steckler, R.; Hu, W.-P.; Liu, Y.-P.; Lynch, G. C.; Garrett, B. C.; Isaacson, A. D.; Lu, D.-H.; Melissas, V. S.; Truong, T. N.; Rai, S. N.; Hancock, G. C.; Lauderdale, J. G.; Joseph, T.; Truhlar, D. G. *POLYRATE*, Version 7.8.1; University of Minnesota: Minneapolis, 1998. (b) Lu, D.-h.; Truong, T. N.; Melissas, V. S.; Lynch, G. C.; Liu, Y.-P.; Garrett, B. C.; Steckler, R.; Isaacson, A. D.; Rai, S. N.; Hancock, G. C.; Lauderdale, J. G.; Joseph, T.; Truhlar, D. G. *Comput. Phys. Commun.* **1992**, *71*, 235.

(33) Villa, J.; Gonzalez-Lafont, A.; Lluch, J.; Bertran, J. *Mol. Phys*. **1996**, *89*, 633.

(34) (a) Parrinello, M. In *MOTEC: Modern Techniques in Computational Chemistry*; Clementi, E., Ed.; ESCOM: Leiden, 1991; p 833. (b) Gonzalez-Lafont, A.; Truong, T. N.; Truhlar, D. G. *J. Phys. Chem.* **1991**, *95*, 4618.

(35) Schmidt, M. W.; Gordon, M. S.; Dupuis, M. *J. Am. Chem. Soc.* **1985**, *107*, 2585.

(36) (a) Garett, B. C.; Redmon, M. J.; Steckler, R.; Truhlar, D. G.; Baldridge, K. K.; Bartol, D.; Schmidt, M. W.; Gordon, M. S. *J. Phys. Chem.* **1988**, *92*, 1476. (b) Melissas, V. S.; Truhlar, D. G.; Garrett, B.C. *J. Chem. Phys.* **1992**, *96*, 5758.

(37) Chuang, Y.-Y.; Truhlar, D. G. *J. Phys, Chem. A* **1997**, *101*, 3808.

(38) Corchado, J. C.; Espinosa-Garcia, J.; Roberto-Neto, O.; Chuang, Y.-Y.; Truhlar, D. G. *J. Phys Chem. A* **1988**, *102*, 4899.

(39) Truhlar D. G. *J. Comput. Chem.* **1990**, *12*, 266.

(40) Truhlar, D. G.; Isaacson, A. D. *J. Chem. Phys.* **1982**, *77*, 3516.

(41) Chuang, Y.-Y.; Fast, P. L.; Hu, W.-P.; Lynch, G. C.; Liu, Y.-P.; Truhlar, D. G. *MORATE*, Version 7.5; University of Minnesota: Minneapolis, 1997.

(42) (a) Sharkey, P.; Smith, I. W. M. *J. Chem. Soc., Faraday Trans.* **1993**, *89*, 631. (b) Taldukar, R. K.; Mellouki, A.; Gierczak, T.; Barone, S.; Chiang, S.-Y.; Ravishankara, A. R. *Int. J. Chem. Kinet.* **1994,** *26*, 973.

(43) (a) Schmoltner, A. M.; Talukdar, R. K.; Warren, R. F.; Mellouki, A.; Goldfarb, L.; Gierczak, T.; McKeen, S. A.; Ravishankara, A. R. *J. Phys. Chem.* **1993**, *97*, 8976. (b) Hsu, K.-J.; DeMore, W. B. *J. Phys. Chem* **1995**, *99*, 1235.

(44) Kasner, J. H.; Taylor, P. H.; Dellinger, B. *J. Phys. Chem.* **1990**, *94*, 3250.

(45) *CRC Handbook of Chemistry and Physics*, 74th ed.; Lide, D. R., Frederikse, H. P. R., Ed.; CRC Press: Boca Raton, Florida, 1993−1994.

(46) Truhlar, D. G. *J. Chem. Soc., Faraday Trans.* **1994**, *90*, 1740.